Chemical and structural induced ductile-to-brittle transition in electrospun silica nanofiber membranes

Bianca Swanckaert[a], Olivier Verschatse[a], Eva Loccufier[a], Klaartje De Buysser[b], Lode Daelemans[a,*], Karen De Clerck[a,*]

[a] *Centre for Textile Science and Engineering (CTSE), Department of Materials, Textiles and Chemical Engineering (MaTCh), Faculty of Engineering and Architecture Ghent University, Technologiepark 70a, 9052 Ghent, Belgium*

[b] *Sol-gel Centre for Research on Inorganic Powders and Thin Films (SCRiPTS), Department of Chemistry, Faculty of Sciences Ghent University, Krijgslaan 281 S3, 9000 Ghent, Belgium*

*Corresponding authors: Lode.Daelemans@UGent.be; Karen.DeClerck@UGent.be

ABSTRACT

Electrospun silica nanofiber membranes show a high potential in many advanced environmental applications. However, little is known about their mechanical performance which could be a limiting factor for further innovation. It is shown in this work that silica nanofiber membranes have a completely different deformation behavior compared to conventional polymeric/thermoplastic nanofiber membranes, resulting from their significant differences in chemical and physical properties such as fiber interactions and porosity. Furthermore, storage at room temperature initiates remarkable changes in failure mechanisms, depending on the storage humidity, which can be accelerated via a thermal treatment. These changes are linked to the structural changes of the membrane resulting from its chemical reactivity towards moisture in the air. Additional interactions and crosslinks are observed, leading to fiber shrinkage and rearrangement. As a result, more contact points are created between nanofibers, creating additional friction forces and, as such, a complete shift in mechanical properties towards a stronger, stiffer, and more brittle material (tensile strength of 14.0 ± 3.8 MPa vs. 3.1 ± 0.4 MPa and failure strain of 0.9 ± 0.2% vs. 24.2 ± 1.0%). The silica nanofiber membranes thus allow mechanical tunability via altering the storage or treatment conditions.

KEYWORDS

Silica nanofiber membranes, electrospinning, sol-gel, deformation behavior, dynamic

HIGHLIGHTS

- Electrospun silica nanofiber membranes show a completely different deformation behavior compared to conventional thermoplastic (PA6) nanofiber membranes
- A mechanical shift is observed in silica nanofiber membranes, depending on the treatment conditions
- The mechanical shift can be linked to structural changes resulting from its chemical reactivity
- Shrinkage and an increase in areal density are observed, leading to more fiber contact points
- Mechanical tunability is possible through treatment conditions

GRAPHICAL ABSTRACT

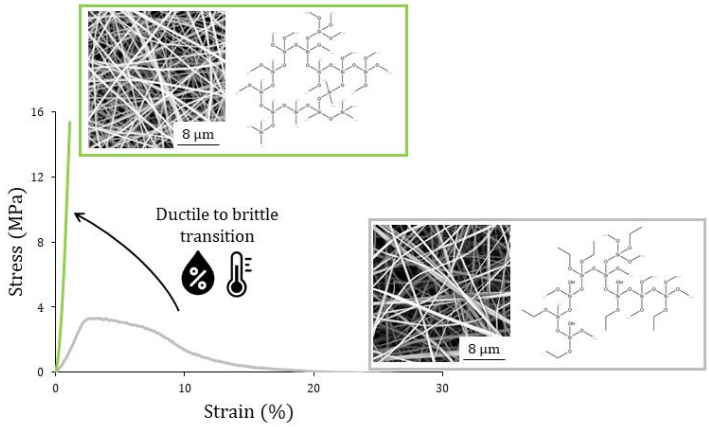

1. *Introduction*

Nanofiber membranes are attractive materials in view of many advanced applications such as microfiltration, separation, and catalysis. Nanofibers typically have a submicron diameter and are generally produced via a method called electrospinning [1]–[3]. This process results in the formation of randomly oriented nanofibers in the form of a non-woven membrane. Due to the specific morphology of these nanofibers, the electrospun membranes have some interesting properties such as high porosity, interconnected pores, and high specific surface area [4]–[6]. As such, nanofiber membranes from e.g. polyamide (PA) are already widely used for water and gas filtration [7]–[11]. While most research has focused on polymeric nanofibers in the past, great attention is currently being given to inorganic nanofibers [12]–[14]. Inorganic nanofibers offer the advantages of a higher thermal and chemical resistance than most polymeric nanofibers [12]. Additionally, via the direct electrospinning of a sol-gel mixture, chemically tunable nanofibers can be produced, resulting in inorganic nanofiber membranes with a wide range of properties and a broad potential application field [15]–[17].

A material with a high potential in this field is silica due to its abundant availability and low cost. Traditionally, silica nanofibers have been produced via electrospinning a sol-gel mixture combined with an organic polymer [13], [18]. This organic polymer allows for better control of the flow behavior during electrospinning. However, when the organic polymer is removed via a thermal treatment afterwards to obtain purely inorganic fibers, the nanofibers have bad mechanical properties [19]. Alternatively, our research group showed a production process for silica nanofiber membranes via direct electrospinning of a sol without organic polymer, resulting in dense inorganic nanofibers with a high purity and better coherency [20], [21]. This is the result of proper control of the reaction mechanisms during the sol-gel synthesis. This synthesis starts from a precursor, tetraethylorthosilicate (TEOS), which reacts with water during a hydrolysis reaction to form silanols in the presence of an acidic catalyst and a homogenizing solvent like ethanol (EtOH). The formed silanols further react via polycondensation reactions to form siloxanes resulting in a cross-linked 3D network (Figure 1) [22]–[25]. Upon controlling these reactions, a TEOS-based electrospinnable sol is formed.

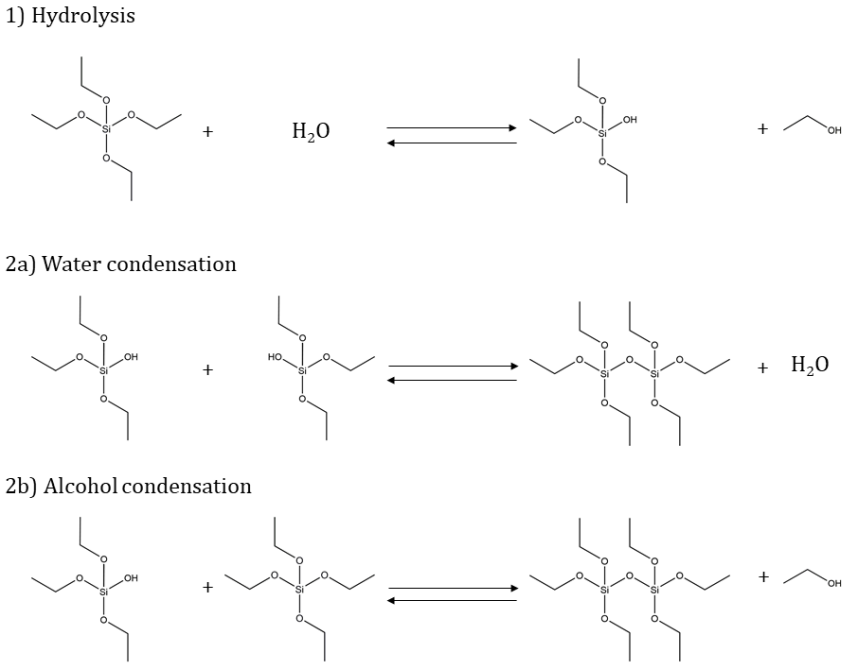

Figure 1: Elementary reactions taking place during the sol-gel synthesis.

It is to be noted that due to incomplete hydrolysis and polycondensation during the sol-gel synthesis, the obtained network is not pure silica yet. Some unhydrolyzed ethoxy and reactive silanol groups are present after electrospinning. These are unstable over time, causing a membrane with dynamic properties. For example, after electrospinning a highly hydrophobic membrane is obtained. However, after storage for some time, a shift occurs to hydrophilic behavior due to further hydrolysis and condensation of the silica structure with moisture in air. The higher the relative humidity of the surrounding air, the faster this shift takes place. A thermal treatment can even further accelerate this shift, and induces additional crosslinks [26]. This dynamic chemical behavior offers many advantages for advanced applications, but the membranes often also require good and predictable mechanical behavior. Due to the dynamic behavior of the chemical structure in silica nanofiber membranes produced via direct electrospinning of a sol, it is expected that this can also have an influence on the mechanical properties of the membranes, as crosslinks are usually linked to an improved mechanical strength [27]–[30].

Traditional silica materials (e.g. glass) are known to have a brittle failure mechanism [31], [32]. A dynamic brittle-to-ductile mechanical behavior has already been observed in some cases. This is most often initiated by physical conditions such as elevated temperature and/or high pressure [33]–[35]. Additionally, the same shift is also observed in silica glass nanofibers, showing a size-effect dependency with brittle behavior for diameters > 18 nm and a strong shift to ductile behavior for diameters < 18 nm [30], [36]. However, for electrospun silica nanofibers via the sol-gel synthesis route, the amount of research on mechanical characterization is limited [19]. It is known that the deformation behavior of electrospun nanofibers can be very complex and many researchers have developed models and simulations to understand the mechanisms taking place [37]–[40]. Our previous work showed that conventional polymeric nanofiber membranes such as PA6 have a high ductility and there are many cohesion forces allowing the membrane to deform as a whole, which is similar as its bulk material [41]. The question remains whether these silica nanofiber membranes will also show similar behavior as its brittle bulk material, or if the nanofiber structure allows for a different deformation mechanism. In addition, the influence of the dynamic chemical nature on their physical and mechanical properties is currently unknown. Gaining more insight into the mechanisms inducing these dynamic properties can help in understanding the material better and to design silica nanofiber membranes with optimal mechanical robustness for advanced applications.

In this research, the mechanical performance of electrospun silica nanofiber membranes is investigated. First, the deformation behavior is studied for an as-spun (untreated) silica nanofiber membrane and compared with a conventional polymeric nanofiber membrane (e.g. PA6). Additionally, the influences of a humidity and thermal treatment on the mechanical properties of the as-spun silica nanofiber membrane are investigated and linked with their chemical and physical nature. It is showcased that there is indeed a shift in deformation behavior as a result of the dynamic chemical nature. An in-depth study with a.o. in-situ scanning electron microscopy (SEM) testing

is performed to understand the underlying mechanisms leading to this dynamic behavior. It is observed that the electrospun silica nanofiber membranes show a strong increase in strength and stiffness after exposure to storage conditions at 65% relative humidity (RH) at room temperature or a thermal treatment at 250-500 °C.

2. Materials and Methods

2.1 Materials

For the production of silica nanofiber membranes, TEOS (≥ 99%, Sigma Aldrich), EtOH (≥ 99.8%, VWR) and hydrochloric acid (HCl, 37%, Sigma Aldrich) were used.

2.2 Methods

2.2.1 Production of silica nanofiber membranes

Prior to electrospinning, the silica network is formed during a sol-gel synthesis. For this, TEOS, EtOH, H_2O and HCl are mixed with molar ratios of 1, 2, 2, 0.01, respectively. TEOS is first mixed with EtOH in an open beaker. Additionally, the H_2O:HCl mixture is added dropwise while vigorously stirring. Afterwards, the temperature is increased to 80 °C and the reaction is proceeded until around $3/8^{th}$ of the volume remains. During the sol-gel synthesis, the viscosity of the solution increases and this was measured using a Brookfield viscometer LVDV-II. Once a viscosity of 110-200 mPa s was reached, the reaction was stopped and could be electrospun on a rotating drum collector at room temperature for several hours (max 6) before the viscosity becomes too high. The flow rate was set at 1 mL h^{-1}, a voltage of 20 kV was applied and the needle-to-collector distance was set at 15 cm. The electrospinning process was performed for 2 hours and nanofiber membranes with an areal density of ± 10 g m^{-2} were produced.

2.2.2 Mechanical testing of nanofiber membranes

Tensile tests were performed using a small tensile tester (TA Instruments Dynamic Mechanical Analysis (DMA) Q800) with a loadcell of 18 N and a strain rate of 1% min^{-1}. The ASTM D882 Standard for Tensile Properties of Thin Plastic Sheeting was used as inspiration during tensile testing. Samples with a gauge length of 20 mm and width of 7 mm were tested. To prevent clamp failure, the region of clamping was reinforced by gluing the nanofiber membranes in between pieces of paper. The cross-section of the samples was calculated based on the mass and density of the membranes to eliminate the contribution of the pores to the cross-section (Eq. 1), as proposed by the study of Maccaferri *et al.* [37]. Since measurement of membrane thickness is unreliable for porous materials, the tensile test data was normalized using the sample mass. Based on their extensive study on a universal approach for tensile testing nanofiber membranes, this method was stated as the most reliable. A mass density of 2.20 g cm^{-3} was used for (amorphous) silica. This is an approximation using the density of the bulk material, since the density of the fiber materials is unknown. The cross-section is then equal to the cross-section of an equivalent solid material where no pores are present, since only the contribution of the solid fibers is relevant. Because of this normalization scheme through an equivalent solid material, different electrospun non-wovens can be quantitively compared with each other.

$$A = \frac{m_{membrane}}{\rho_{silica} * l} \qquad \text{Eq. 1}$$

With $m_{membrane}$ the mass of the nanofiber membrane, ρ_{silica} its corresponding density (approximated as 2.20 g cm^{-3} for bulk amorphous silica) and l the length of the sample. For each membrane, three samples were tested. The tensile tests were performed 48 hours after electrospinning, unless mentioned otherwise. Additionally, the porosity (ε) was determined via Eq. 2.

$$\varepsilon = 1 - \frac{m_{membrane}/\rho_{silica}}{w * l * t} \qquad \text{Eq. 2}$$

With w the width and t the thickness of the membranes, measured with a precision micrometer. Note that measurements of the thickness with a precision meter is unreliable for porous materials, as mentioned before, and was therefore performed to calculate an estimation of the porosity only and not the membrane cross sectional area. For testing the dynamic behavior over time, silica nanofiber membranes were stored in climatized rooms of either 25 ± 2% RH or 65 ± 4% RH. Each week, tensile tests were performed on both membranes for a period of six weeks. Additionally, the silica nanofiber membranes were also thermally treated at 250 °C, 400 °C and 500 °C for one hour (and three hours at 250 °C) using a Muffle Furnace from Nabertherm GmbH. The chemical changes were analyzed using attenuated total reflection Fourier transform infrared (ATR-FTIR, Nicolet iS50 FT-IR setup with OMNIC software) in the range 400-4000 cm^{-1}. The spectra were normalized with respect to the Si-O-Si signal at 1076 cm^{-1}.

2.2.3 In-situ microscopy during mechanical testing

To investigate the deformation and failure behavior of the silica nanofiber membranes on a microscopic scale, in-situ microscopy was used. First, the tensile tests were monitored using a digital optical microscope (DinoLite AM4515ZTL). Additionally, tensile tests were also performed in-situ using Scanning Electron Microscopy (SEM). For this, a Phenom XL tensile stage was used with a dedicated loadcell of 150 N (Deben). Samples were first coated with a gold layer of 10 nm. The tensile test was performed stepwise (steps of 0.02 mm), with a high quality SEM image taken at each step. A small incision was made in the samples to predict the area of failure. The in-situ SEM tensile tests were performed on samples with a gauge length of 10 mm and a width of 7 mm. Physical properties such as area were measured via a micrometer.

3. Results and discussion

3.1 Deformation behavior of untreated silica nanofiber membranes

The untreated as-spun silica nanofiber membrane shows a remarkable mechanical behavior (Figure 2 black curve). A strong brittle failure behavior with high stiffness is expected for silica based on its general bulk properties. However, this is not observed in the case of the as-spun silica nanofiber membranes. There is a clear elastic region until the ultimate tensile strength (UTS) is reached, which is in accordance with brittle behavior. Once the UTS is reached, a region of slow decline is observed. This is the result of nanofibers unraveling from the membrane, leading to high failure strains. However, the initial crack is formed at the UTS, and thus the additional strain is completely related to the fibers moving and reorienting out of the crack opening along the tensile direction. This behavior is also observed for classical non-woven materials that show under-bonding [42]. This indicates that there is almost no cohesion (due to e.g. friction forces) present in the as-spun silica nanofiber membrane, allowing a lot of individual fiber movements and failure at very low forces. Note that the mechanical properties obtained by the normalization scheme will never be equal to that of a solid bulk material as they represent the aggregated response of the non-woven membrane. As stated by the theories of cellular solids, a clear relationship exists between the Young's modulus of a porous material and its relative density (= ratio of density of the cellular solid and density of the bulk material), similarly as observed in the case of the non-woven membrane [43], [44]. On the contrary, a PA6 nanofiber membrane shows clear Poisson contraction prior to failure (Figure 2 red curve) resulting in a ductile deformation behavior. There is almost no fiber movement in the vicinity of the crack on a macroscopic scale because the PA6 nanofiber membrane has a lot of cohesion in its structure, resulting in much more transfer of forces [41]. Additionally, the as-spun silica nanofiber membrane has a lower stiffness than expected from its bulk material, and the UTS is significantly lower than the PA6 nanofiber membrane (Table 1). These observations can also be linked to the porosity of the membranes. A higher porosity is observed for the as-spun silica nanofiber membrane compared to PA6 due to its bigger fiber diameter (Table 1, Figure 3), indicating that there are less contact points between fibers [37], [45], [46]. As contact points are the main contributor for friction forces in nanofiber membranes, lower forces are observed for the as-spun silica. Additionally, a comparison was made between the as-spun silica nanofiber membranes from this work and silica nanofiber membranes produced with the aid of a sacrificial organic polymer during electrospinning. As mentioned before, there is only limited amount of research available on the mechanical performance of silica nanofiber membranes, and since an organic polymer is used during electrospinning, the available data only shows the mechanical performance after calcination (Table 1). Contrary, in this work, a thorough study of the mechanical performance of silica nanofiber membranes produced via the direct electrospinning of a sol without sacrificial organic polymer was performed for the first time which gives more insight into the relationship between the chemical, structural and mechanical properties.

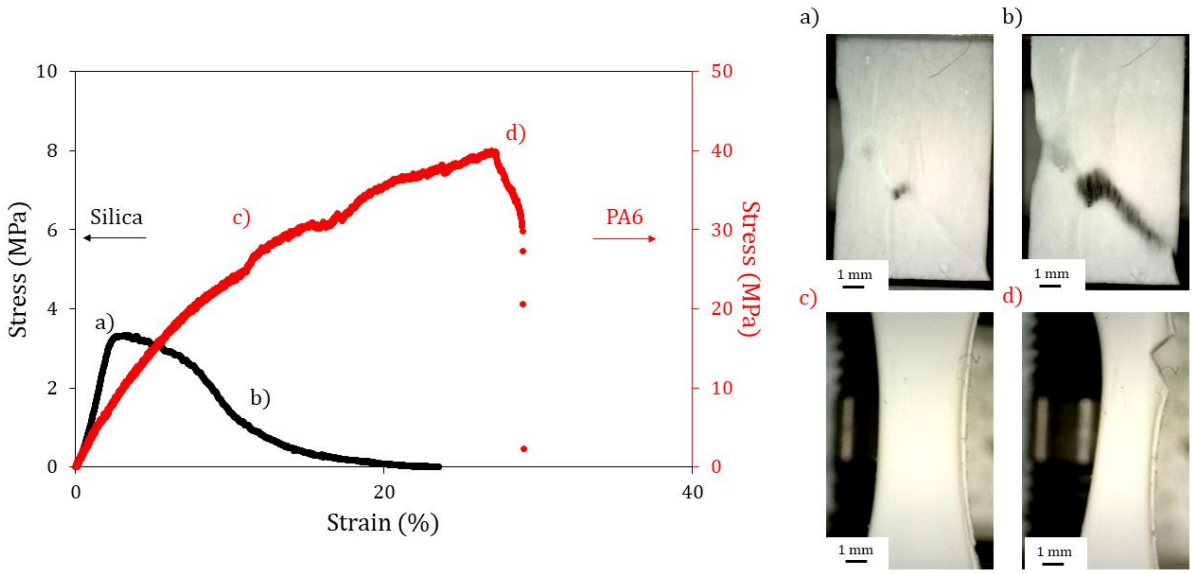

Figure 2: Results of tensile tests on an untreated as-spun silica nanofiber membrane (tested at a strain rate of 1% min^{-1}), compared to a PA6 nanofiber membrane from our previous work [41] with their corresponding failure mechanisms. The images are taken during the tensile tests at points a), b), c) and d) as shown on the stress-strain curves.

Table 1: Mechanical properties of PA6 and untreated silica nanofiber membranes during a tensile test.

	UTS (MPa)	**Failure strain (%)**	**E (MPa)**	**Porosity (%)**	**REF**
PA6 nanofiber membrane	38.5 ± 6.0	30.0 ± 2.8	370 ± 34	81.5 ± 1.0	[41]
As-spun silica nanofiber membrane	3.1 ± 0.4	24.2 ± 1.0	184 ± 36	96.4 ± 0.8	This work
Silica nanofiber membrane (calcinated)	0.5-4.5	0.5-6.5	-	-	[47]

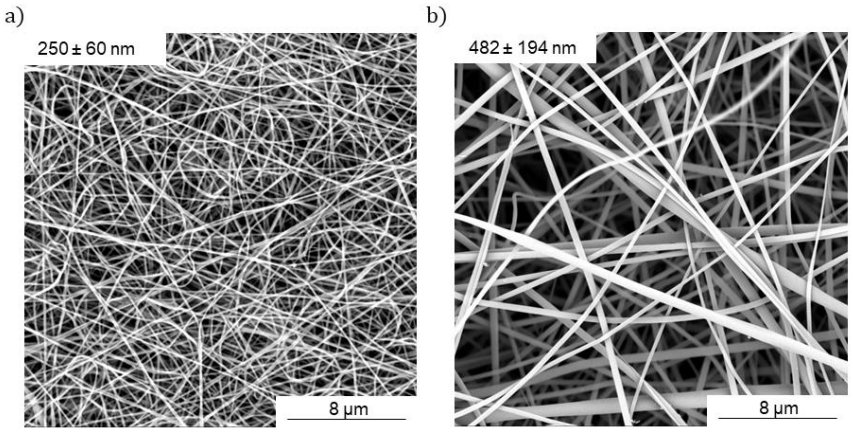

Figure 3: SEM images of a) PA6 nanofibers and b) untreated as-spun silica nanofibers with their corresponding fiber diameter.

More detailed insights into the deformation behavior of as-spun silica nanofiber membranes are obtained via in-situ SEM tensile testing (Figure 4). A small incision perpendicular to the tensile direction was made prior to testing to locate the crack region. It was observed that the crack propagates from this incision, with complete alignment of the fibers to the tensile direction. There is almost no fiber failure (Figure 4b) and the large failure strains result from very large unraveling lengths of no less than 960 µm in the case of the in-situ tensile test. This indicates that the observed stress-strain behavior from Figure 2 entirely relates to the membrane structure, with movement and

reorientation of the brittle silica nanofibers. Little to no cohesion between the nanofibers is observed, resulting in a very low UTS and stiffness.

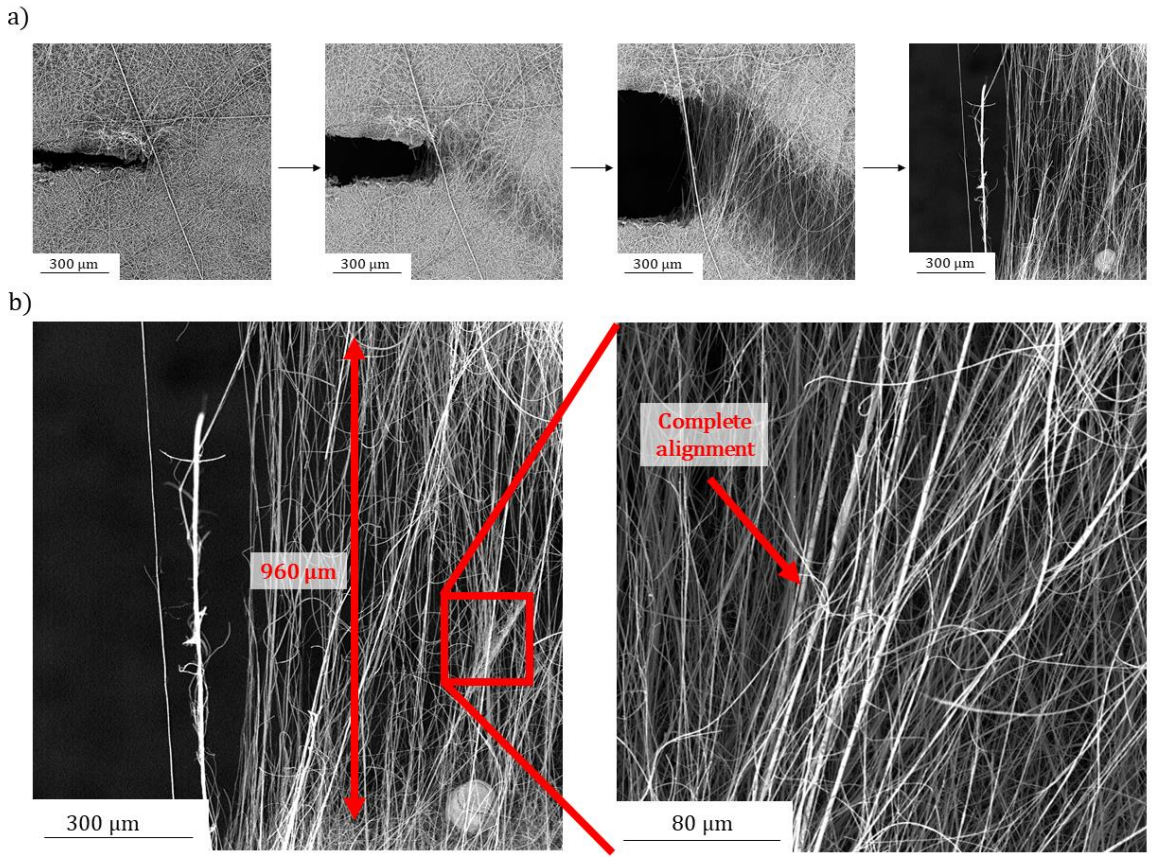

Figure 4: Snapshots during in-situ SEM tensile testing on untreated as-spun silica nanofiber membranes, a) showing large fiber unraveling areas. Focus at the crack propagation zone in b) shows complete alignment of the fibers, with an unravelling length of no less than 960 µm.

3.2 Dynamic mechanical behavior: influence of humidity and thermal treatment

Tensile tests were performed on the silica nanofiber membranes over a course of 43 days, during storage at 25% RH and 65% RH, to investigate the changes in mechanical behavior upon applying a humidity treatment (Figure 5). In both cases, a remarkable shift is observed, going from a membrane with large failure strains prior to treatment, to a stronger and more brittle behavior after ageing. This shift is highly dependent on the storage conditions. While the failure strain already drops from 23.4 ± 1.6% to 1.2 ± 0.0% after 1 week at 65% RH, at 25% RH it takes 3 to 4 weeks to complete this shift (Figure 5b). Additionally, the UTS has increased from 2.9 ± 0.5 MPa to 11.1 ± 2.6 MPa at 65% RH but only to 4.6 ± 1.9 MPa at 25% RH after 43 days (Figure 5a). It thus appears that the changes in mechanical behavior are strongly influenced by the storage conditions, and occur faster at a higher relative humidity treatment.

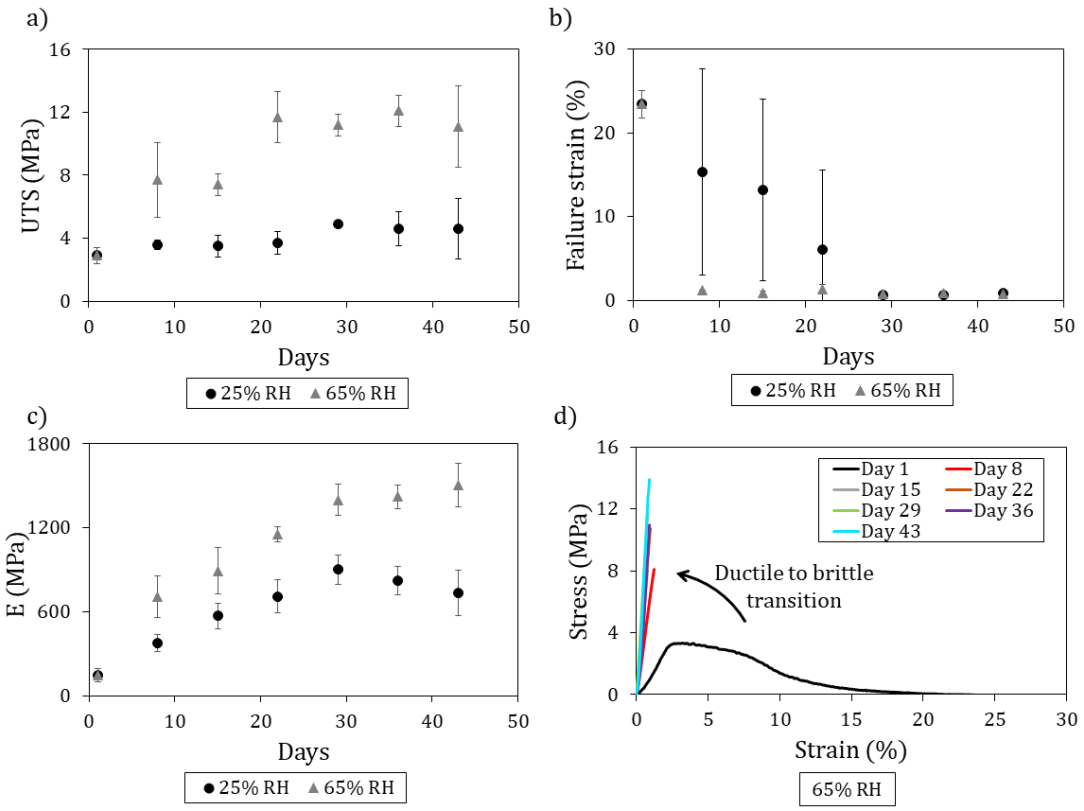

Figure 5: Evolution of a) UTS, b) failure strain and c) E for an as-spun silica nanofiber membrane stored at different relative humidities. d) Stress-strain curves over time for a membrane stored at 65% RH show a clear ductile to brittle transition.

Since it is known that the chemical structure also changes upon applying a thermal treatment, tensile tests were also performed after several thermal treatments (Figure 6). At 250 °C, the changes in mechanical behavior are limited, but the failure mechanisms show a bigger shift as the thermal treatment duration increases. However, even after 3 hours the UTS is still relatively low. At temperatures of 400 °C and 500 °C, the same changes are observed as during storage at RT. However, it appears that a treatment of 1 hour is in these cases already enough to induce a complete shift in mechanical behavior. At 500 °C a UTS of 14.0 ± 3.8 MPa is observed, which is 4.6 times higher than the initial UTS of an untreated as-spun silica nanofiber membrane, with a failure strain of 0.9 ± 0.2% (Figure 6a and 6b). It is clear that the temperature during a thermal treatment strongly influences the speed and extent of the shift in mechanical behavior.

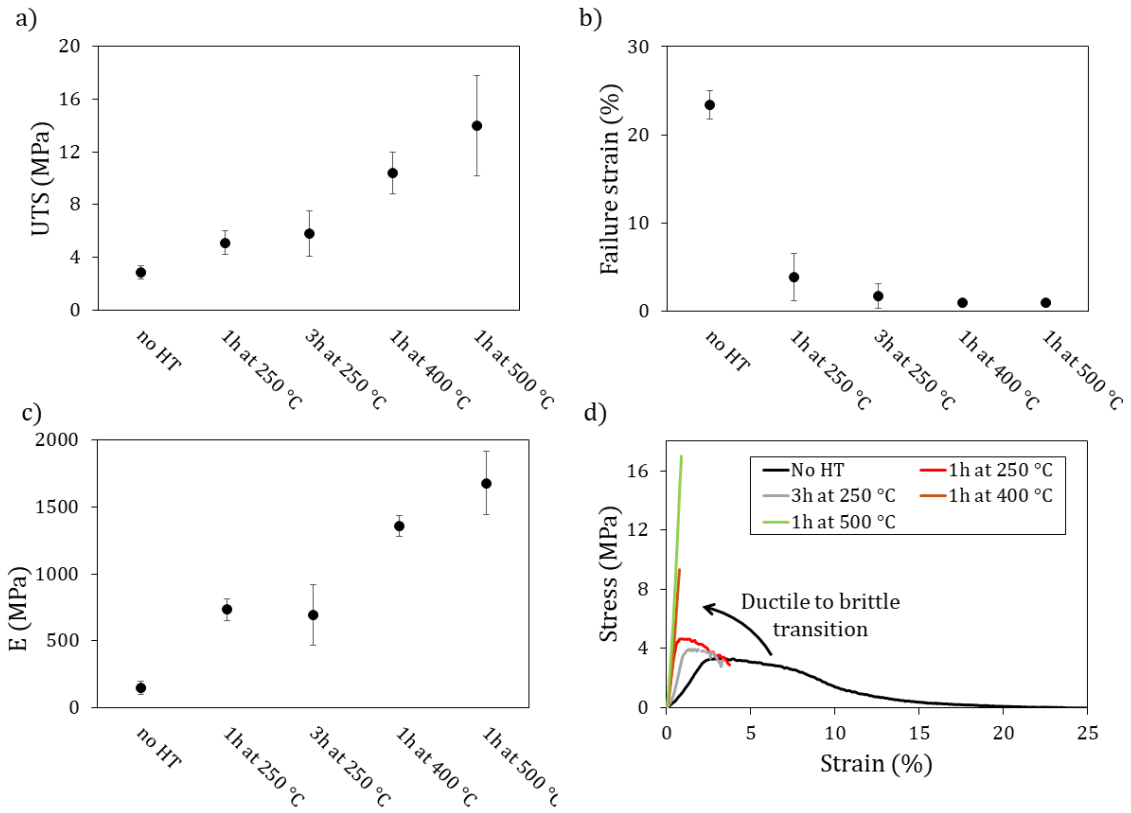

Figure 6: Evolution of a) UTS, b) failure strain and c) E for an as-spun silica nanofiber membrane receiving different thermal treatments. d) Example of corresponding stress-strain curves, showing a clear transition from ductile to brittle after a thermal treatment. Note that there is a clear temperature dependency.

In-situ tensile testing after a thermal treatment for 1 hour at 400 °C shows that the treated silica nanofiber membrane fails in a more brittle way (Figure 7). There is a clear crack in the failure region, and many fibers break immediately upon loading, with thus a smaller amount of fibers reorienting themselves along the tensile direction compared to the untreated as-spun membrane (Figure 4). A complete alignment of the fibers remains absent, resulting in an unraveling length in the case of the in-situ tensile test of only 240 µm (Figure 7b) compared to 960 µm for the untreated membrane (note that these specimens have a small incision to facilitate crack initiation). These results and observations indicate that fiber movement has become more restricted in the membranes that underwent a humidity or thermal treatment. Fibers are also observed to break before they can fully align according to the tensile direction.

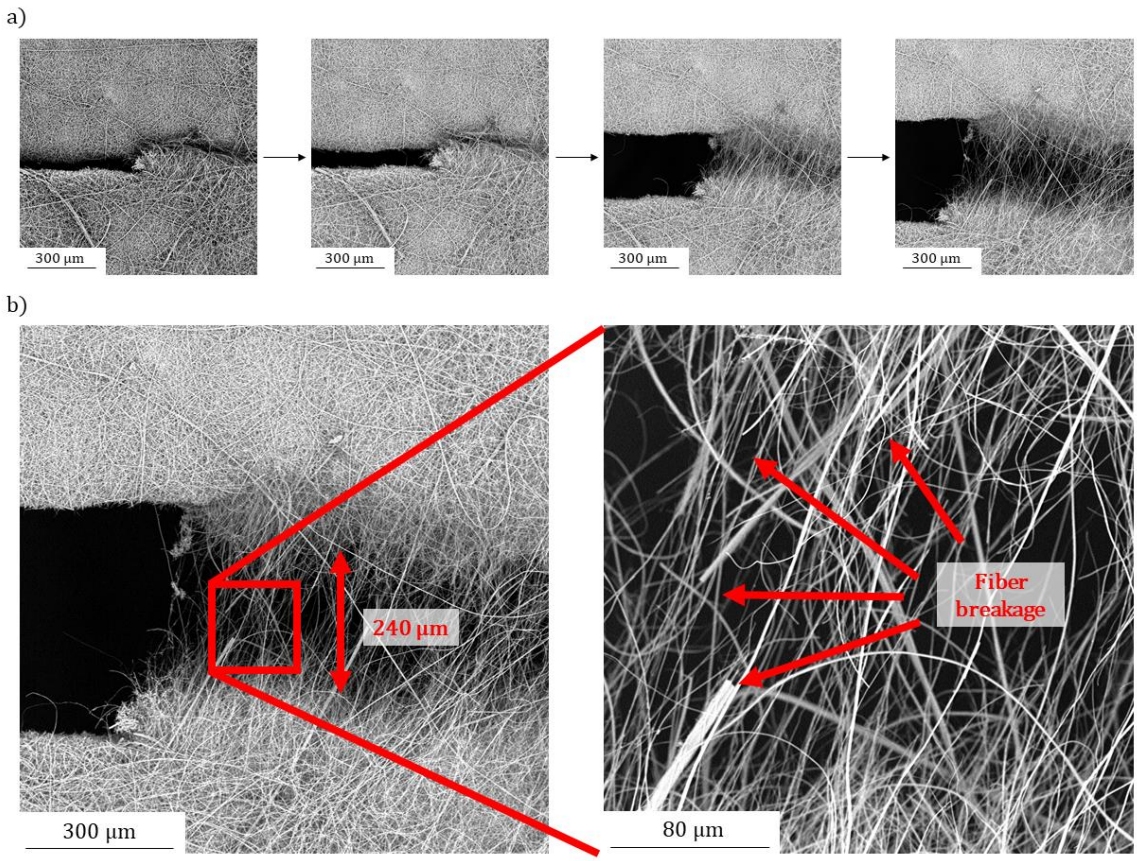

Figure 7: a) In-situ SEM tensile test of treated silica nanofiber membranes after a thermal treatment for 1 hour at 400 °C. b) A much smaller unraveling length is observed with many fibers that are broken.

3.3 Changes in chemical structure of the treated silica nanofiber membranes

It is clear that there are two very distinctive microscopic deformation behaviors that can be detected for these silica nanofiber membranes, depending on the treatment conditions. This results in significant differences in mechanical properties on a macroscopic scale, with both mechanical behaviors very different compared to traditional polymeric nanofiber membranes. To investigate the underlying mechanisms for this shift in behavior, the evolution of the chemical and physical properties upon applying these treatments are analyzed.

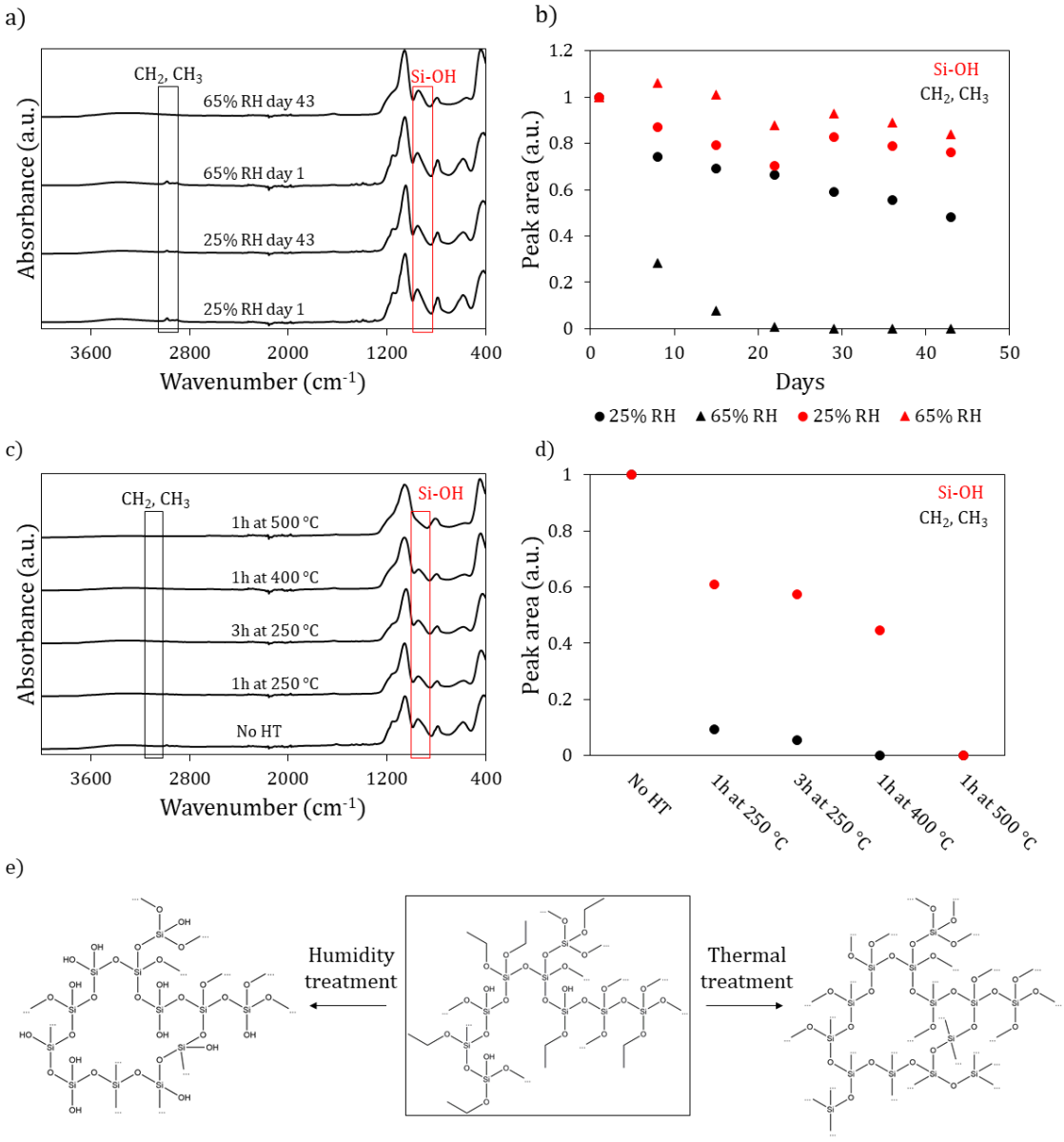

Figure 8: a) ATR-FTIR evolution of as-spun silica nanofiber membranes stored at 25% RH or 65% RH for 43 days. b) The evolution of peak surface area is shown for CH_2, CH_3 (3020-2850 cm^{-1}) and Si-OH (966 cm^{-1}) [48]. c) ATR-FTIR evolution during several thermal treatments, with d) the evolution of their peak surface area. e) Schematics of the chemical changes observed via ATR-FTIR. All spectra were normalized with respect to the O-Si-O signal at 1055 cm^{-1}.

ATR-FTIR measurements before and after the humidity treatments were done show a decline in CH_3, CH_2 signals (3020-2850 cm^{-1}) over time. This is accelerated by exposure to a higher RH (Figure 8a and 8b), with a removal of 52% at 25% RH and a removal of 100% at 65% RH after 43 days. This is due to hydrolysis reactions taking place in the membrane structure with moisture in the air resulting in a substitution of ethoxy groups by hydroxyl groups (Figure 8e). It is observed that the signals corresponding to Si-OH (966 cm^{-1}) do not show that same clear decrease which would be expected when cross-linking via polycondensation occurs (a removal of 24% at 25% RH and a removal of 16% at 65% RH after 43 days). However, the hydrolysis reaction leads to an increase in silanol while the condensation simultaneously leads to a decrease in silanol, resulting in a less straightforward evolution over time. This is in line with previous research which has proven that there is indeed additional cross-linking over time, albeit limited [26].

The same ATR-FTIR analyses after several thermal treatments show again a very steep decrease of CH_2, CH_3 with a complete removal at temperatures ≥ 400 °C (Figure 8c and 8d). Additionally, a significant decrease in silanol groups is also observed, and the decrease gets bigger with higher temperatures (a removal of 40% at 1h at 250 °C,

43% at 3h at 250 °C, 55% at 1h at 400 °C and 100% at 1h at 500 °C). This proves that there is indeed additional cross-linking within the silica network since silanols react to form siloxane bonds (Figure 8e).

Overall, a dynamic behavior is observed in chemical structure for membranes receiving a humidity treatment and membranes receiving a thermal treatment. Despite evolving towards the same brittle and stronger mechanical behavior, the chemical changes are slightly different for both treatments, as schematically depicted in 2D in Figure 8e. At RT, the changes are predominated by hydrolysis and (some) condensation reactions, similarly as during the sol-gel synthesis of the silica network prior to electrospinning. As a result, the network evolves towards a structure which gets slightly more cross-linked over time and which contains many silanol groups. Alternatively, during a thermal treatment the ethoxy groups are completely removed and almost all silanol groups condensate into a highly cross-linked structure, depending on the temperature. In both cases, additional interactions are formed due to the crosslinks and hydrogen bonds from the silanol groups. This is expected to result in an increased stiffness and strength of the individual fibers, with a more brittle behavior.

3.4 Changes in physical properties of the treated silica nanofiber membranes

A last important consideration are the physical changes of the membranes upon applying various treatments, such as area and areal density (determined as mass divided through the corresponding area). In all cases, areal shrinkage was observed, with an increasing areal density (Figure 9). However, the areal density has a slower incline because there is some mass loss associated to the previously described chemical changes. At RT during storage at 25% RH and 65% RH, the shrinkage has a slower evolution at lower humidity, in line with the evolution in chemical changes (Figure 9a and 9b). In this case, the large amount of silanol groups in the structures at RT results in an increased amount of hydrogen bond interactions leading to a more closely packed structure resulting in shrinkage and rearrangement (e.g. bending) of the fibers within the membrane [49], [50]. SEM images of the nanofiber membranes confirm the increase in amount of fibers for the same surface area after storage (Figure 10). As a consequence, there are more contact points between the fibers for a same surface area, which is associated to a higher strength due to more friction forces and fiber-fiber interactions taking place.

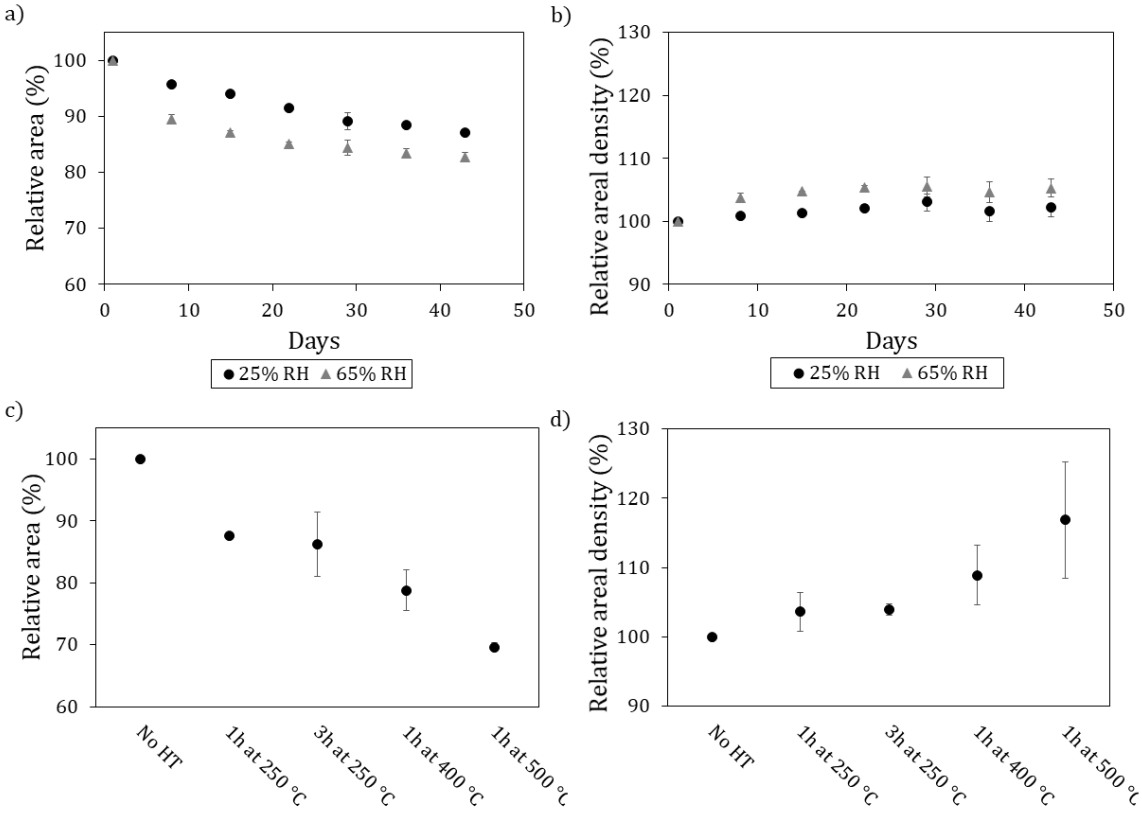

Figure 9: Relative area and relative areal density of as-spun silica nanofiber membranes during storage at 25% RH and 65% RH (a and b), and during different thermal treatments (c and d). At RT, the properties were determined by comparing them against day 1. For the thermal treatments, the properties were determined by comparing each sample before and after the corresponding thermal treatment.

During a thermal treatment, the same changes in physical properties are observed and are also in line with the chemical and mechanical changes (Figure 9c and 9d). In this case, the formation of additional cross-links within the fibers results in a more closely packed chemical structure with rearrangement of the fibers and shrinking of the membrane as a consequence. In all cases, this areal shrinkage and rearrangement results in more fibers and additional contact points with fiber-fiber interactions between different fibers for the same surface area. Several interactions can take place at these contact points such as chemical crosslinks, hydrogen bonds and physical interactions leading to more friction forces and a reduction of the individual fiber mobility. It is generally known that fiber-fiber interactions lead to significant changes in mechanical properties [51]–[53]. SEM images of the nanofiber membranes confirm the increase in amount of fibers for the same surface area after thermal treatment (Figure 10). As a result, a strong increase in UTS is observed in all cases, with a bigger effect depending on the treatment conditions, and since silica is inherently brittle, a more brittle failure behavior is observed for the nanofiber membrane as well. Analysis of the fiber diameters before and after treatment revealed no significant changes in fiber diameter, except for 43 days at 65% RH. However, this is most likely a consequence of the electrospinning process and the measuring technique, both introducing variation in the results.

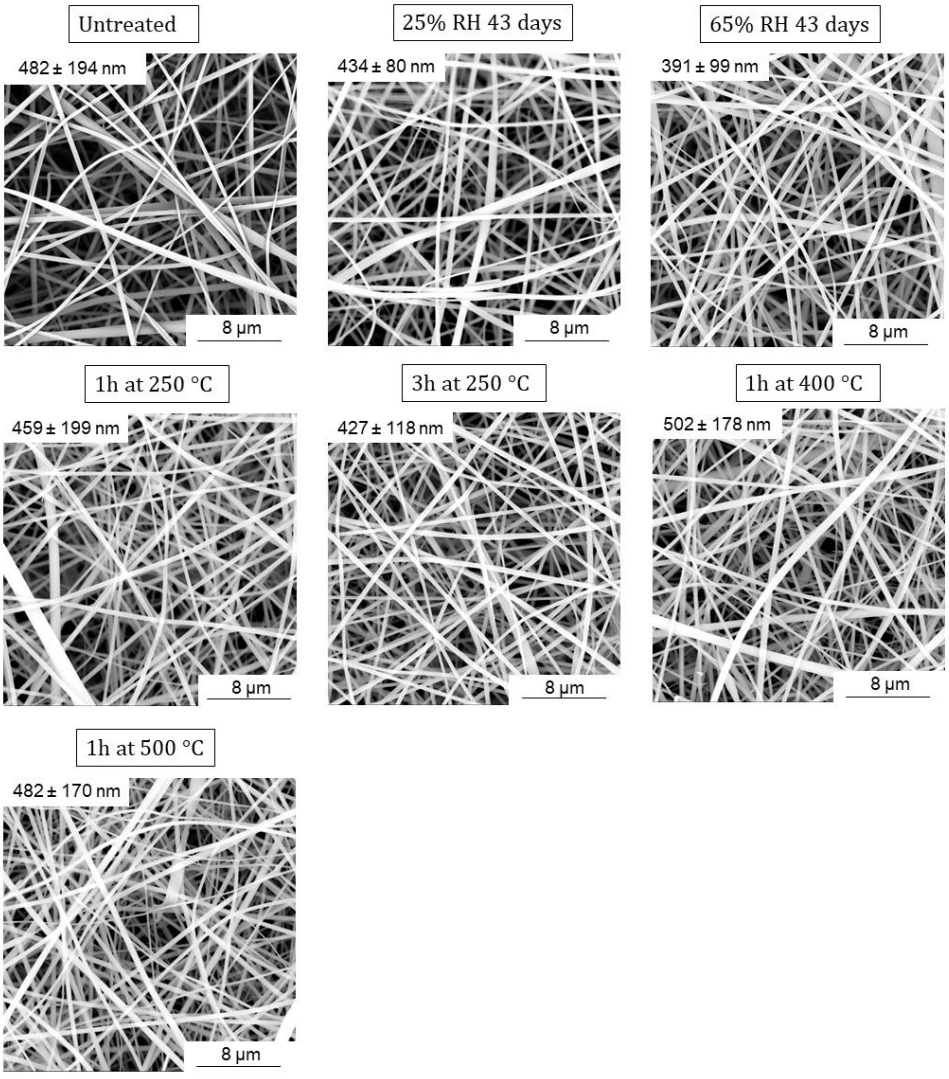

Figure 10: SEM images showing the increase in amount of fibers for a same surface area after humidity or thermal treatment.

It is clear that the chemical changes resulting from the dynamic structure of the as-spun silica nanofiber membranes thus induce physical changes such as areal shrinkage on a macroscopic scale, resulting in a strong shift in mechanical properties due to additional contact between the fibers. However, it remains unclear if this observed shrinkage during thermal treatment is purely resulting from changes in chemical structure, since thermal tensions can also lead to physical changes of materials.

To assess the cause of the shrinkage, the thermal treatment at 400 °C was monitored over time during which every 5 minutes a sample was removed and analyzed. Again, there were no morphological changes and no significant changes in fiber diameter observed during the thermal treatment (Supporting information Figure S1). Already after 5 minutes at 400 °C, a shrinkage of almost 20% and an increase in areal density of ± 10% are observed, which did not significantly increase over time during the course of 1 hour thermal treatment (Figure 11a and 11b). However, ATR-FTIR analysis reveals that the chemical changes as mentioned before also already occur after 5 minutes at 400 °C with no additional significant changes during the remaining course of 1 hour thermal treatment (Figure 11c). As expected, this is again linked with the mechanical performance of the silica nanofiber membranes, with a shift towards a brittle behavior already after 5 minutes as well (Figure 11d, 11e and 11f). However, the stiffness still increases after 5 minutes, indicating that the shift had not been completed yet. It is clear that the chemical and physical changes observed in the nanofiber membrane are directly linked with each other and are responsible for the changes in mechanical performance regardless of the treatment conditions.

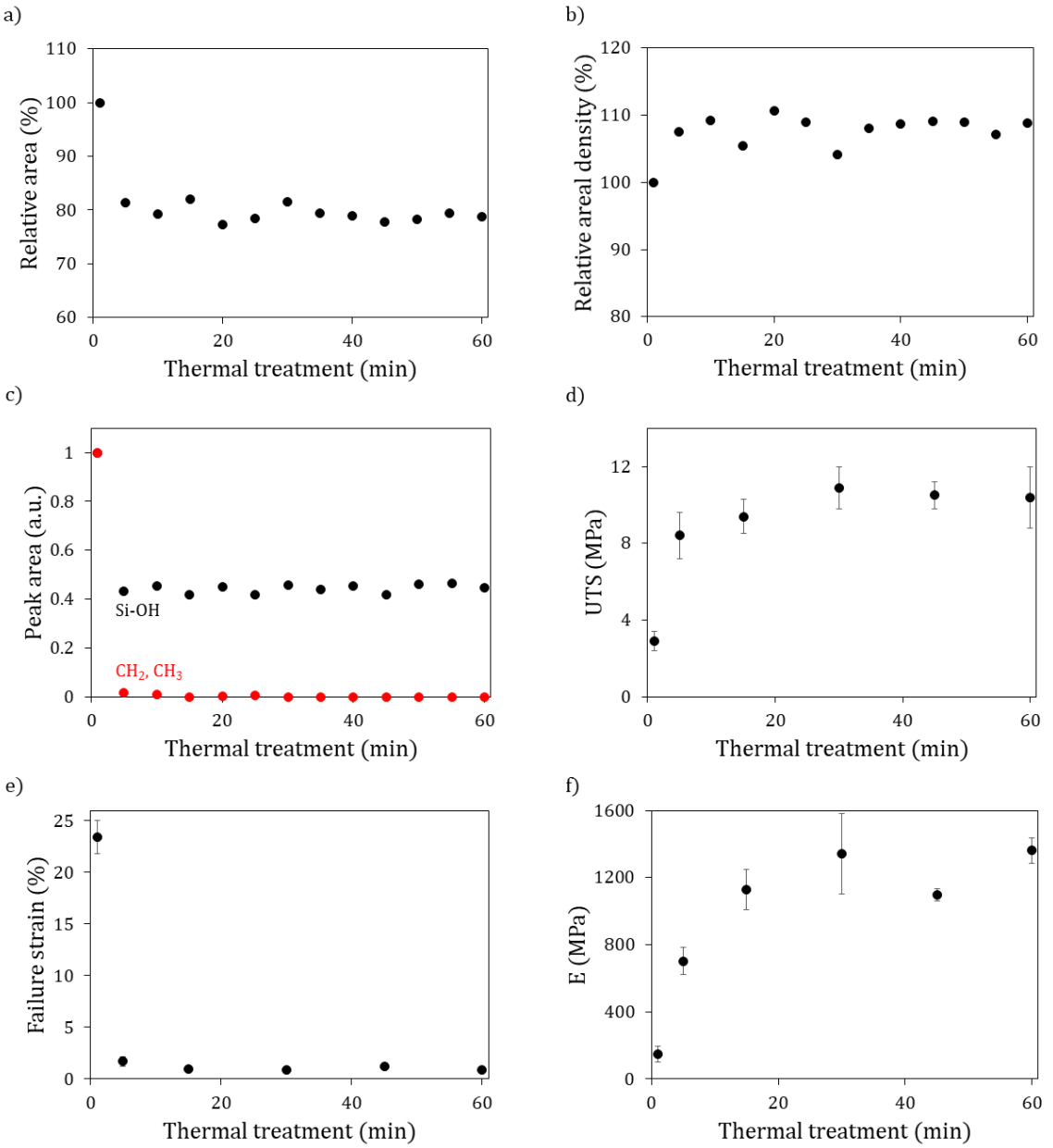

Figure 11: Changes in a) area, b) surface density, c) ATR signals, d) UTS, e) failure strain and f) E of a silica nanofiber membrane during a thermal treatment at 400 °C during 1 hour. For each point in time, analyses were performed on one membrane of which three samples were cut to perform tensile testing.

4. Conclusion

The mechanical behavior of directly electrospun silica nanofiber membranes was investigated. First, a clear difference was observed between the behavior of an as-spun silica and PA6 nanofiber membrane. This originates from differences in interactions and contact points between the fibers, resulting in more friction forces for PA6 nanofiber membranes. Additionally, a remarkable shift in failure mechanism was observed for the as-spun silica nanofiber membrane, originating from specific treatment conditions such as high humidity storage or thermal treatment. This shift originates from changes in chemical nature of the nanofibers, leading to additional interactions such as hydrogen bonds and crosslinks. This in turn results in physical changes such as membrane shrinkage creating additional contact points and fiber-fiber interactions between the nanofibers for the same surface area. As such, more friction forces are present and an increase in strength and stiffness is observed. However, since the fiber-fiber interactions reduce the fiber mobility, the treated silica nanofiber membrane reaches its failure strain more quickly due to the brittle nature of silica. It is clear that directly electrospun silica nanofiber membranes can be mechanically tuned by altering the treatment conditions. This is a direct consequence of the production method via the direct electrospinning of a silica sol. Not only does this allow to chemically tune the nanofibers, but it was now proven that they can also be mechanically tuned.

ACKNOWLEDGEMENTS

The Research Foundation – Flanders (FWO) is gratefully acknowledged by B.S. for funding the research through an SB PhD grant (1S84322N). L.D. and K.D.C acknowledge the financial support of Ghent University, in specific the project grant BOF/STA/202009/046 and BOF19/24J/102, respectively.

[1] S. Ramakrishna, K. Fujihara, W. E. Teo, T. Yong, Z. Ma, and R. Ramaseshan, “Electrospun nanofibers: Solving global issues,” *Mater. Today*, vol. 9, no. 3, pp. 40–50, 2006, doi: 10.1016/S1369-7021(06)71389-X.

[2] D. Li and Y. Xia, “Electrospinning of nanofibers: Reinventing the wheel?,” *Adv. Mater.*, vol. 16, no. 14, pp. 1151–1170, 2004, doi: 10.1002/adma.200400719.

[3] J. Xue, J. Xie, W. Liu, and Y. Xia, “Electrospun Nanofibers: New Concepts, Materials, and Applications,” *Acc. Chem. Res.*, vol. 50, no. 8, pp. 1976–1987, 2017, doi: 10.1021/acs.accounts.7b00218.

[4] F. E. Ahmed, B. S. Lalia, and R. Hashaikeh, “A review on electrospinning for membrane fabrication: Challenges and applications,” *Desalination*, vol. 356, pp. 15–30, 2015, doi: 10.1016/j.desal.2014.09.033.

[5] A. Barhoum, K. Pal, H. Rahier, H. Uludag, I. S. Kim, and M. Bechelany, “Nanofibers as new-generation materials: From spinning and nano-spinning fabrication techniques to emerging applications,” *Appl. Mater. Today*, vol. 17, pp. 1–35, 2019, doi: 10.1016/j.apmt.2019.06.015.

[6] J. Xue, T. Wu, Y. Dai, and Y. Xia, “Electrospinning and electrospun nanofibers: Methods, materials, and applications,” *Chem. Rev.*, vol. 119, no. 8, pp. 5298–5415, 2019, doi: 10.1021/acs.chemrev.8b00593.

[7] J. Matulevicius, L. Kliucininkas, D. Martuzevicius, E. Krugly, M. Tichonovas, and J. Baltrusaitis, “Design and characterization of electrospun polyamide nanofiber media for air filtration applications,” *J. Nanomater.*, vol. 2014, 2014, doi: 10.1155/2014/859656.

[8] P. Heikkilä, A. Taipale, M. Lehtimäki, and A. Harlin, “Electrospinning of Polyamides With Different Chain Compositions for Filtration Application,” *Polym. Eng. Sci.*, pp. 1168–1176, 2008, doi: 10.1002/pen.

[9] S. Yan, Y. Yu, R. Ma, and J. Fang, “The formation of ultrafine polyamide 6 nanofiber membranes with needleless electrospinning for air filtration,” *Polym. Adv. Technol.*, vol. 30, no. 7, pp. 1635–1643, 2019, doi: 10.1002/pat.4594.

[10] J. Avossa, T. Batt, T. Pelet, S. P. Sidjanski, K. Schönenberger, and R. M. Rossi, “Polyamide Nanofiber-Based Air Filters for Transparent Face Masks,” *ACS Appl. Nano Mater.*, vol. 4, no. 11, pp. 12401–12406, 2021, doi: 10.1021/acsanm.1c02843.

[11] G. Yin, Q. Zhao, Y. Zhao, Y. Yuan, and Y. Yang, “The electrospun polyamide 6 nanofiber membranes used as high efficiency filter materials: Filtration potential, thermal treatment, and their continuous production,” *J. Appl. Polym. Sci.*, vol. 128, no. 2, pp. 1061–1069, 2013, doi: 10.1002/app.38211.

[12] D. Malwal and P. Gopinath, “Fabrication and applications of ceramic nanofibers in water remediation: A review,” *Crit. Rev. Environ. Sci. Technol.*, vol. 46, no. 5, pp. 500–534, 2016, doi: 10.1080/10643389.2015.1109913.

[13] H. Wu, W. Pan, D. Lin, and H. Li, “Electrospinning of ceramic nanofibers: Fabrication, assembly and applications,” *J. Adv. Ceram.*, vol. 1, no. 1, pp. 2–23, 2012, doi: 10.1007/s40145-012-0002-4.

[14] Y. Peng *et al.*, “Strong Flexible Ceramic Nanofiber Membranes for Ultrafast Separation of Oil Pollutants,” *ACS Appl. Nano Mater.*, vol. 5, no. 7, pp. 9389–9400, 2022, doi: 10.1021/acsanm.2c01681.

[15] S. Sakai, K. Kawakami, and M. Taya, “Controlling the Diameters of Silica Nanofibers Obtained by Sol-Gel/Electrospinning Methods,” *J. Chem. Eng. JAPAN*, vol. 45, no. 6, pp. 436–440, 2012, doi: 10.1252/jcej.11we249.

[16] S. Choi and S. G. O. O. Lee, “Silica nanofibers from electrospinning/sol-gel process,” *J. Mater. Sci. Lett.*, vol. 22, pp. 891–893, 2003.

[17] B. Swanckaert *et al.*, “Sulfonated silica-based cation-exchange nanofiber membranes with superior self-cleaning abilities for electrochemical water treatment applications,” *Sep. Purif. Technol.*, vol. 309, no. November 2022, p. 123001, 2023, doi: 10.1016/j.seppur.2022.123001.

[18] T. Pirzada, S. A. Arvidson, C. D. Saquing, S. S. Shah, and S. A. Khan, “Hybrid Silica − PVA Nanofibers via Sol − Gel Electrospinning,” 2012.

[19] Y. Si, X. Mao, H. Zheng, J. Yu, and B. Ding, “Silica nanofibrous membranes with ultra-softness and

enhanced tensile strength for thermal insulation," *RSC Adv.*, vol. 5, no. 8, pp. 6027–6032, 2015, doi: 10.1039/c4ra12271b.

[20] J. Geltmeyer, L. Van Der Schueren, F. Goethals, K. De Buysser, and K. De Clerck, "Optimum sol viscosity for stable electrospinning of silica nanofibres," *J. Sol-Gel Sci. Technol.*, vol. 67, no. 1, pp. 188–195, 2013, doi: 10.1007/s10971-013-3066-x.

[21] J. Geltmeyer, J. De Roo, F. Van den Broeck, J. C. Martins, K. De Buysser, and K. De Clerck, "The influence of tetraethoxysilane sol preparation on the electrospinning of silica nanofibers," *J. Sol-Gel Sci. Technol.*, vol. 77, no. 2, pp. 453–462, 2016, doi: 10.1007/s10971-015-3875-1.

[22] A. M. Buckley and M. Greenblatt, "The Sol-Gel Preparation of Silica Gels," *J. Chem. Educ.*, vol. 71, no. 7, pp. 599–602, 1994.

[23] J. Livage, F. Beteille, C. Roux, M. Chatry, and P. Davidson, "Sol-gel synthesis of oxide materials," *Acta Mater.*, vol. 46, no. 3, pp. 743–750, 1998, doi: 10.1016/S1359-6454(97)00255-3.

[24] J. Livage and C. Sanchez, "Sol-gel chemistry," *J. Non. Cryst. Solids*, vol. 145, no. C, pp. 11–19, 1992, doi: 10.1016/S0022-3093(05)80422-3.

[25] S. Verschraegen *et al.*, "A dedicated protocol to capture orthosilicate crosslinking kinetics and Arrhenius parameters," *Chem. Eng. J.*, vol. 461, no. February, p. 141701, 2023, doi: 10.1016/j.cej.2023.141701.

[26] E. Loccufier, J. Geltmeyer, L. Daelemans, D. R. D'hooge, K. De Buysser, and K. De Clerck, "Silica Nanofibrous Membranes for the Separation of Heterogeneous Azeotropes," *Adv. Funct. Mater.*, vol. 28, no. 44, pp. 1–10, 2018, doi: 10.1002/adfm.201804138.

[27] W. Wang *et al.*, "Effect of vapor-phase glutaraldehyde crosslinking on electrospun starch fibers," *Carbohydr. Polym.*, vol. 140, pp. 356–361, 2016, doi: 10.1016/j.carbpol.2015.12.061.

[28] Y. Z. Zhang, J. Venugopal, Z. M. Huang, C. T. Lim, and S. Ramakrishna, "Crosslinking of the electrospun gelatin nanofibers," *Polymer (Guildf).*, vol. 47, no. 8, pp. 2911–2917, 2006, doi: 10.1016/j.polymer.2006.02.046.

[29] H. Tian *et al.*, "Electrospinning of polyvinyl alcohol into crosslinked nanofibers: An approach to fabricate functional adsorbent for heavy metals," *J. Hazard. Mater.*, vol. 378, no. June, p. 120751, 2019, doi: 10.1016/j.jhazmat.2019.120751.

[30] J. Luo *et al.*, "Size-Dependent Brittle-to-Ductile Transition in Silica Glass Nanofibers," *Nano Lett.*, vol. 16, no. 1, pp. 105–113, 2016, doi: 10.1021/acs.nanolett.5b03070.

[31] J. Sehgal and S. Ito, "Brittleness of glass," *J. Non. Cryst. Solids*, vol. 253, no. 1–3, pp. 126–132, 1999, doi: 10.1016/S0022-3093(99)00348-8.

[32] T. P. Swiler, J. H. Simmons, and A. C. Wright, "Molecular dynamics study of brittle fracture in silica glass and cristobalite," *J. Non. Cryst. Solids*, vol. 182, no. 1–2, pp. 68–77, 1995, doi: 10.1016/0022-3093(94)00546-X.

[33] T. Rouxel and J. C. Sanglebœuf, "The brittle to ductile transition in a soda-lime-silica glass," *J. Non. Cryst. Solids*, vol. 271, no. 3, pp. 224–235, 2000, doi: 10.1016/S0022-3093(00)00109-5.

[34] J. Samuels and S. G. Roberts, "The brittle-ductile transition in silicon. I Experiments," *Proc. R. Soc. A*, vol. 421, no. 1860, pp. 1–23, 1988.

[35] F. Yuan and L. Huang, "Brittle to ductile transition in densified silica glass," *Sci. Rep.*, vol. 4, pp. 1–8, 2014, doi: 10.1038/srep05035.

[36] S. Bonfanti, E. E. Ferrero, A. L. Sellerio, R. Guerra, and S. Zapperi, "Damage Accumulation in Silica Glass Nanofibers," *Nano Lett.*, vol. 18, no. 7, pp. 4100–4106, 2018, doi: 10.1021/acs.nanolett.8b00469.

[37] E. Maccaferri *et al.*, "How Nanofibers Carry the Load: Toward a Universal and Reliable Approach for Tensile Testing of Polymeric Nanofibrous Membranes," *Macromol. Mater. Eng.*, vol. 306, no. 7, 2021, doi: 10.1002/mame.202100183.

[38] A. Kulachenko and T. Uesaka, "Direct simulations of fiber network deformation and failure," *Mech. Mater.*, vol. 51, pp. 1–14, 2012, doi: 10.1016/j.mechmat.2012.03.010.

[39] X. Wei, Z. Xia, S. C. Wong, and A. Baji, “Modelling of mechanical properties of electrospun nanofibre network,” *Int. J. Exp. Comput. Biomech.*, vol. 1, no. 1, p. 45, 2009, doi: 10.1504/ijecb.2009.022858.

[40] M. Zhang, W. Lu, P. I. Gouma, Z. Xu, and L. Wang, “Theoretical prediction of effective stiffness of nonwoven fibrous networks with straight and curved nanofibers,” *Compos. Part A Appl. Sci. Manuf.*, vol. 143, no. January, p. 106311, 2021, doi: 10.1016/j.compositesa.2021.106311.

[41] O. Verschatse, E. Loccufier, B. Swanckaert, K. De Clerck, and L. Daelemans, “Microscale and Macroscale Deformation Behavior of Electrospun Polymeric Nanofiber Membranes Using In Situ SEM during Mechanical Testing,” 2023.

[42] B. Pourdeyhimi and B. Maze, *Structure and mechanics of nonwovens*. Woodhead Publishing Limited, 2008.

[43] M. F. Ashby, “Mechanical Properties of Cellular Solids.,” *Metall. Trans. A, Phys. Metall. Mater. Sci.*, vol. 14 A, no. 9, pp. 1755–1769, 1983, doi: 10.1007/BF02645546.

[44] A. P. Roberts and E. J. Garboczi, “Elastic moduli of model random three-dimensional closed-cell cellular solids,” *Acta Mater.*, vol. 49, no. 2, pp. 189–197, 2001, doi: 10.1016/S1359-6454(00)00314-1.

[45] S. J. Eichhorn and W. W. Sampson, “Statistical geometry of pores and statistics of porous nanofibrous assemblies,” *J. R. Soc. Interface*, vol. 2, no. 4, pp. 309–318, 2005, doi: 10.1098/rsif.2005.0039.

[46] S. J. Eichhorn and W. W. Sampson, “Relationships between specific surface area and pore size in electrospun polymer fibre networks,” *J. R. Soc. Interface*, vol. 7, no. 45, pp. 641–649, 2010, doi: 10.1098/rsif.2009.0374.

[47] Y. Yu, “Silica ceramic nanofiber membrane with ultra-softness and high temperature insulation,” *J. Mater. Sci.*, vol. 57, pp. 4080–4091, 2022, doi: 10.1007/s10853-022-06913-6.

[48] B. C. Smith, *Infrared spectral interpretation : a systematic approach*. Boca Raton (Fla.) : CRC press, 1999.

[49] I. S. Chuang and G. E. Maciel, “A detailed model of local structure and silanol hydrogen bonding of silica gel surfaces,” *J. Phys. Chem. B*, vol. 101, no. 16, pp. 3052–3064, 1997, doi: 10.1021/jp9629046.

[50] I-Ssuer Chuang and and G. E. Maciel, “Probing Hydrogen Bonding and the Local Environment of Silanols on Silica Surfaces via Nuclear Spin Cross Polarization Dynamics,” *J. Am. Chem. Soc.*, vol. 118, no. 2, pp. 401–406, 1996, doi: 10.1021/ja951550d.

[51] S. Buell, G. C. Rutledge, and K. J. V. Vliet, “Predicting polymer nanofiber interactions via molecular simulations,” *ACS Appl. Mater. Interfaces*, vol. 2, no. 4, pp. 1164–1172, 2010, doi: 10.1021/am1000135.

[52] Y. You, S. W. Lee, S. Jin Lee, and W. H. Park, “Thermal interfiber bonding of electrospun poly(L-lactic acid) nanofibers,” *Mater. Lett.*, vol. 60, no. 11, pp. 1331–1333, 2006, doi: 10.1016/j.matlet.2005.11.022.

[53] K. B. Yilmaz, B. Sabuncuoglu, B. Yildirim, and V. V. Silberschmidt, “A brief review on the mechanical behavior of nonwoven fabrics,” *J. Eng. Fiber. Fabr.*, vol. 15, 2020, doi: 10.1177/1558925020970197.